

## GRAVITATIONAL WAVE SIGNATURES IN BLACK-HOLE-FORMING CORE COLLAPSE

PABLO CERDÁ-DURÁN, NICOLAS DEBRYE, MIGUEL A ALOY, JOSÉ A FONT AND MARTIN OBERGAULINGER  
Departamento de Astronomía y Astrofísica, Universidad de Valencia, c/ Dr. Moliner, 50, 46100 - Burjassot, Spain  
*Draft version August 30, 2018*

### ABSTRACT

We present numerical simulations in general relativity of collapsing stellar cores. Our initial model consists of a low metallicity rapidly-rotating progenitor which is evolved in axisymmetry with the latest version of our general relativistic code CoCoNuT, which allows for black hole formation and includes the effects of a microphysical equation of state (LS220) and a neutrino leakage scheme to account for radiative losses. The motivation of our study is to analyze in detail the emission of gravitational waves in the collapsar scenario of long gamma-ray bursts. Our simulations show that the phase during which the proto-neutron star (PNS) survives before ultimately collapsing to a black hole is particularly optimal for gravitational wave emission. The high-amplitude waves last for several seconds and show a remarkable quasi-periodicity associated with the violent PNS dynamics, namely during the episodes of convection and the subsequent nonlinear development of the standing-accretion shock instability (SASI). By analyzing the spectrogram of our simulations we are able to identify the frequencies associated with the presence of g-modes and with the SASI motions at the PNS surface. We note that the gravitational waves emitted reach large enough amplitudes to be detected with third-generation detectors as the Einstein Telescope within a Virgo cluster volume at rates  $\lesssim 0.1 \text{ y}^{-1}$ .

*Subject headings:* gravitational waves — stars: massive — supernovae: general — black hole physics

### 1. INTRODUCTION

The collapse of the core of a massive and rotating star is the most likely mechanism to generate central engines suitable to explain the huge energy output inferred from long lasting gamma-ray bursts (GRBs) (Woosley 1993). One of the theoretical requisites to produce a viable engine for GRBs is that a central black hole (BH) forms with a mass  $\geq 3 M_{\odot}$  surrounded by a thick accretion disk. During the formation of the BH-accretion disk system, a low-density funnel shall also form along the rotational axis of the system, to provide a suitable least-resistance region for any ultrarelativistic outflow to escape without accumulating an excessive amount of baryonic mass. The path followed by the collapsing core until it forms a GRB central engine was early devised by MacFadyen & Woosley (1999) and MacFadyen et al. (2001). More recently, (O'Connor & Ott 2011; DeBrye et al. 2013) have argued that BH formation in a massive stellar core is almost always preceded by the formation of a proto-neutron star (PNS) which may last for  $\sim 0.8$  s.

The formation of BHs in massive stars is typically associated with electromagnetic counterparts which are dimmer than typical core collapse supernovae (SNe) (Horiuchi et al. 2011; Woosley & Heger 2012; Kochanek 2013), and with failed SNe or unnovae (Lovegrove & Woosley 2013; Piro 2013). Zhang et al. (2008) estimate the fraction of supernova-like compact remnants that can be produced by fall back mechanisms, finding that the least energetic explosions experience more fall back and, hence, produce more massive remnants. Indeed, Zhang et al. (2008) estimate that, leaving aside any influence of rotation and binary membership of the progenitor star, the fraction of remnants that will be BHs can be up to  $\sim 90\%$ . In a more sophisticated numer-

ical setting, Ugliano et al. (2012) conclude that  $\sim 23\%$  of the potential massive progenitors with solar-metallicity end up as BHs. Fryer et al. (2012) point out that it is difficult to make a strong SN explosion if there is a long delay between shock formation and the convective phase of typical convection-enhanced, neutrino-driven engines. If the explosion occurs less than 250 ms after bounce, SN energies in excess of  $10^{51}$  erg are expected.

In this work we consider the process of BH formation by means of 2D general relativistic numerical simulations and focus on the gravitational wave (GW) signature imprinted by the process of formation of GRB central engines for progenitor systems with subsolar metallicity ( $Z = 0.1 Z_{\odot}$ ) and various rotational profiles. We will show that together with neutrino signals, the unique GW signature of the process with durations of a few seconds makes the delayed formation of rotating BHs from massive stellar progenitors excellent targets for the next generation of GW surveys.

### 2. SETUP

Our numerical simulations of the collapse of rapidly rotating stellar cores are performed using the CoCoNuT code (Dimmelmeier et al. 2002, 2005), that solves the general relativistic hydrodynamics equations in a dynamically evolved space-time, using the XCFC approximation (Cordero-Carrión et al. 2009). The progenitor is a  $35 M_{\odot}$  star at zero-age main-sequence from (Woosley & Heger 2006) with high initial rotation rate and low metallicity (model 35OC). The model has lost about  $7 M_{\odot}$  due to strong winds and has an iron core of  $2.02 M_{\odot}$  in its pre-supernova stage with  $\sim 2 \text{ rad s}^{-1}$  central angular velocity. The iron core mass of this model is among the largest in stellar evolution computations (Woosley et al. 2002; Woosley & Heger 2006; Chieffi & Limongi 2013). We evolve the innermost  $22 M_{\odot}$  of the progenitor using spherical polar coordinates

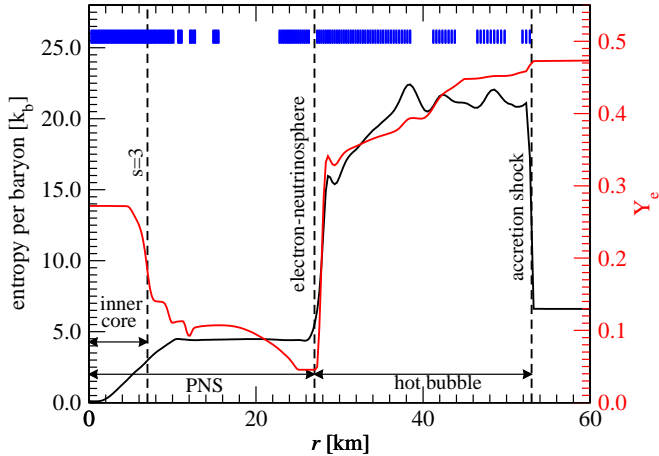


FIG. 1.— Radial profile of the entropy per baryon (black-solid line, left scale) and electron fraction (red-solid line, right scale) at the equator, 497.5 ms after bounce showing typical conditions inside the shock. Blue bars show radial extension of convectively stable regions.

with  $n_r \times n_\theta = 1200 \times 64$  grid points for the hydrodynamics. The innermost 20 km are covered with 100 uniformly distributed radial grid points and outwards the radial cells increase to cover the whole domain. We impose axisymmetry and symmetry with respect to the equatorial plane. The field equations are solved using spectral methods with the LORENE library, using 17 radial domains with  $n_r \times n_\theta = 17 \times 9$  collocation points on each.

For the equation of state (EoS) we resort to the table provided by O’Connor & Ott (2010) matching at high densities the EoS of Lattimer & Swesty (1991) with nuclear compressibility  $K = 220$  MeV (LS220 hereafter), and at densities below  $10^8$  g cm $^{-3}$  the EoS of Timmes & Arnett (1999).

During the collapse we employ a deleptonization prescription akin to that of Liebendörfer (2005b), which assumes that the electron fraction at any given time is a single function of the rest-mass density. The profiles used in our simulations have been extracted from 1D non-rotating simulations performed with the code described by Obergaulinger & Janka (2012). Although the progenitor is rotating, during the collapse phase the core preserves its sphericity very closely. Therefore, the spherically symmetric deleptonization scheme should provide a good approximation to the collapse phase.

After bounce, we use a grey neutrino leakage scheme (Ruffert et al. 1996; Rosswog & Liebendörfer 2003; O’Connor & Ott 2010; DeBrye et al. 2013) Opacities and emission rates include nuclear and nucleonic emission/absorption and scattering of neutrinos, electron-positron pair formation and plasmon decay. We compute the optical depth ray-by-ray and define the neutrinospheres for the different neutrino species based on the optical depth. Although our neutrino treatment lacks of energy deposition terms, it should provide a good estimate of the cooling and contraction of the PNS after bounce. In fact it reproduces within 25% the results of Liebendörfer et al. (2005a) (model G15) with full Boltzmann neutrino transport. We extract the GWs by means of the quadrupole formula.

### 3. THE LONG PATH TO BLACK HOLE FORMATION

We have performed two long term simulations with two different initial rotation profiles: a *fiducial simulation*, which uses the original rotation profile of the model 35OC and a relatively *slow rotation simulation*, in which the angular velocity profile is half that of the fiducial.

In the *fiducial simulation* the core collapses in 342.7 ms. At this point a shock forms, which expands rapidly to a radius of  $\sim 130$  km and contracts slowly afterwards. Figure 1 shows the typical conditions found once the accretion shock has formed. A long accretion phase follows in which matter accretes through the stalled shock, heats up due to photo-disintegration of nuclei and piles up on top of the newly formed PNS, the surface of which is determined by the large density gradient located close to the electron neutrinosphere. Hereafter we define the *inner core* as the cold region of unshocked material with entropy per baryon  $s < 3 k_b$  and the PNS as all the matter enclosed in the electron-neutrinosphere. After 1.6 s the PNS becomes unstable to radial perturbations and collapses to a BH. Several processes regulate the time of formation of the BH but they can be summarized in two groups: those controlling the accretion rate, and those modifying the maximum mass supported by the PNS before becoming unstable.

The shock accretion rate is dominated by the outer core initial density profile and by the deleptonization processes cooling the matter outside the shock. Figure 2 shows the time evolution of accreted baryonic mass. The initial accretion rate of baryonic mass exceeds  $1 M_\odot s^{-1}$  and lasts for  $\sim 220$  ms. Afterwards the accretion rate drops dramatically as the less dense layers outside the iron core accrete (DeBrye et al. 2013). At  $\sim 340$  ms after bounce the accretion rate stabilizes to  $0.45 M_\odot s^{-1}$  for the rest of the simulation. Once the accreting matter crosses the stalled shock it heats up and falls through the hot bubble in which the particles can dwell for some time before reaching the surface of the PNS, due to convection and the standing accretion shock instability (SASI). In a failed supernova, the dwell time is bounded between the spherical inward advection time, typically  $\sim 10$  ms, and a time of  $\sim 50$  ms (see, e.g., Figure 17 of Buras et al. (2006)). For much longer dwell times matter should be able to win enough energy from the outstreaming neutrinos to produce a successful explosion. We have checked that the PNS mass follows the mass enclosed in the shock with a delay of  $\sim 50$  ms during the initial fast accretion phase and  $\sim 100$  ms afterwards. Since the dwell time is significantly smaller than the total time for BH formation (1.6 s), the accretion rate onto the PNS is dominated by the events occurring outside of the accretion shock, and not by the details of the complicated microphysics behind the shock. We have compared the accretion rate through the shock for the two different rotation rates finding no significant difference.

Since the maximum gravitational (baryonic) mass supported by LS220 is  $2.04 M_\odot$  ( $2.41 M_\odot$ ), consistent with the recent observation of a  $1.97 \pm 0.04 M_\odot$  neutron star (Demorest et al. 2010), the formation of a BH in a stellar core collapse will not occur in the timescale of the accretion of the iron core, but it will extend generically to timescales longer than  $\sim 0.5$  s (MacFadyen & Woosley 1999). In the collapsar scenario the maximum mass can be modified by effects of rotation and tempera-

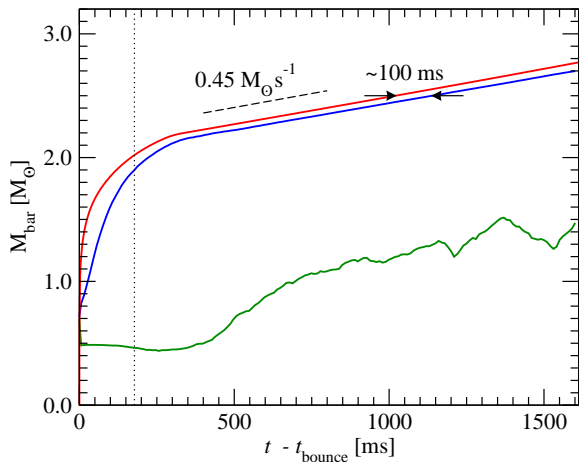


FIG. 2.— Time evolution of the baryonic mass inside the shock (red line), PNS surface (blue line) and inner core (green line). After all the iron core has been accreted (vertical black-dotted line) the accretion rate drops to  $\sim 0.45 M_{\odot} \text{ s}^{-1}$ .

ture. Galeazzi et al. (2013) have estimated that for a LS220 neutron star and similar conditions to our PNS models ( $s = 4 k_b$  and  $\beta$ -equilibrium in their work) the maximum baryon mass decreases by  $\sim 7\%$ . If we restrict to rotation profiles stable against dynamical non-axisymmetric instabilities, differential rotation can easily support neutron stars with baryonic mass above  $3 M_{\odot}$  (Baumgarte et al. 2000; Morrison et al. 2004; Kaplan et al. 2013). In our fiducial (slow rotation) simulation the PNS mass increases up to  $\sim 2.70 M_{\odot}$  ( $2.45 M_{\odot}$ ) before collapsing to BH. It is important to notice that the thermal structure and the rotation profile of the PNS evolves from the time of bounce to the time of BH formation. That means that the maximum mass at the formation of the BH and thus the time for BH formation, depends on the history of the PNS along these  $\sim 1.6$  s of evolution, including the cooling by neutrinos diffusing out of the PNS and the angular momentum redistribution. The presence of strong magnetic fields, due to the magneto-rotational instability, or non-axisymmetric instabilities will probably enhance the transport of angular momentum, decreasing the maximum mass supported by the PNS and hence decreasing the time to BH formation. Therefore, the non-magnetized axisymmetric simulations presented in this work should provide an upper limit to the BH formation time. A lower limit for this model can be estimated as the time at which  $2.41 M_{\odot}$  have accreted through the shock, i.e.  $\sim 820$  ms. Using a stiffer EoS would allow for larger maximum masses and hence longer collapse times.

#### 4. GRAVITATIONAL WAVEFORMS

Due to the rapid rotation (central period  $P_c \sim 1.5$  ms at bounce) the PNS is significantly deformed with a polar-to-equatorial radius ratio of  $\sim 0.64$  after bounce. As accretion proceeds and the PNS cools down and contracts from  $\sim 80$  km at bounce to  $\sim 14$  km at BH formation, it spins up reaching  $P_c \sim 0.48$  ms at BH formation. The activity inside the PNS and in the hot bubble behind the shock is continuously perturbing the strongly deformed star giving rise to a long duration stage of large amplitude GW emission (see Figure 3a). As the PNS contracts the characteristic frequency of the signal

increases. The spectrogram of the signal (Figure 3b) confirms this trend but also shows a rich variety of features, imprints of different processes in the PNS. We have identified the different features in the spectrogram by performing a similar spectrogram of different variables (rest mass density and velocity) at different locations in the star.

The feature labeled “A” shows a monotonic increase of the frequency with time, which can be traced back to the surface of the PNS. A similar pattern was found in core-collapse simulations (Murphy et al. 2009; Müller et al. 2013), which was linked to g-modes on the PNS surface. The analysis of the Brunt-Väisälä frequency shows two convectively stable layers correlated with the positive entropy gradients located at the surface of the PNS and the inner core. Perturbations of these convectively stable layers lead to oscillations with a characteristic buoyancy frequency given by  $f_g \sim \sqrt{N^2}/2\pi$ . Following Müller et al. (2013), the surface of the PNS can be regarded as isothermal and described with an ideal gas EoS of pressure  $P = \rho k_b T / m_n$ , with  $k_b$  the Boltzmann constant,  $m_n$  the neutron mass and  $T$  the temperature of the fluid. Approximating the metric as the Schwarzschild metric in isotropic coordinates the frequency of g-modes at the surface of the PNS can be approximated as

$$f_{g,\text{PNS}} \sim \frac{1}{2\pi} \frac{M_{\text{PNS}}}{R_{\text{PNS}}^2} \left(1 + \frac{M_{\text{PNS}}}{2R_{\text{PNS}}}\right)^{-4} \sqrt{\frac{\Gamma - 1}{\Gamma} \frac{m_n}{k_b T}}. \quad (1)$$

We use  $\Gamma = 4/3$  and  $k_b T = 15$  MeV, which fits closely the increasing frequency behaviour of feature “A” (solid-green line in Figure 3b), since the surface of the PNS contracts and its mass rises with time.

The feature labeled “B” increases in frequency up to  $\sim 1$  kHz and then decreases strongly. We have identified its origin in the inner core. During the rise we recognize velocity patterns in this region with a clear quadrupolar structure. During the quick frequency drop, the velocity pattern becomes quasi-radial, and it ends up with the collapse to a BH. We associate the change in behaviour of this feature during the evolution to an avoided crossing of two modes: i) a g-mode related to the innermost convectively stable layer first, and ii) a quasi-radial mode with decreasing frequency. As the frequency of the quasi-radial mode goes to zero, this mode becomes unstable and the formation of the BH proceeds (Chandrasekhar 1964). This effect has been observed in numerical evolutions of neutron stars around its maximum mass (Gourgoulhon et al. 1995; Galeazzi et al. 2013). Avoided crossings of radial-modes with f-modes (Gondek et al. 1997; Kokkotas & Ruoff 2001) and crustal-modes (Gondek & Zdunik 1999) have been found in linear perturbation analysis. It is reasonable to expect that radial modes and g-modes should show a similar behavior, as our simulations indicate. To model the g-modes in the inner core we assume a constant increase of the entropy per baryon  $\Delta s/s \sim 2$  over the gravity scale height

$$f_{g,c} \sim \frac{1}{2\pi} \frac{M_{\text{IC}}}{R_{\text{IC}}^2} \left(1 + \frac{M_{\text{IC}}}{2R_{\text{IC}}}\right)^{-4} \sqrt{\frac{1}{\Gamma} \frac{\Delta s}{s}}, \quad (2)$$

with  $\Gamma = 2.6$ .  $M_{\text{IC}}$  and  $R_{\text{IC}}$  correspond to the contribution to the gravitational mass enclosed in the inner

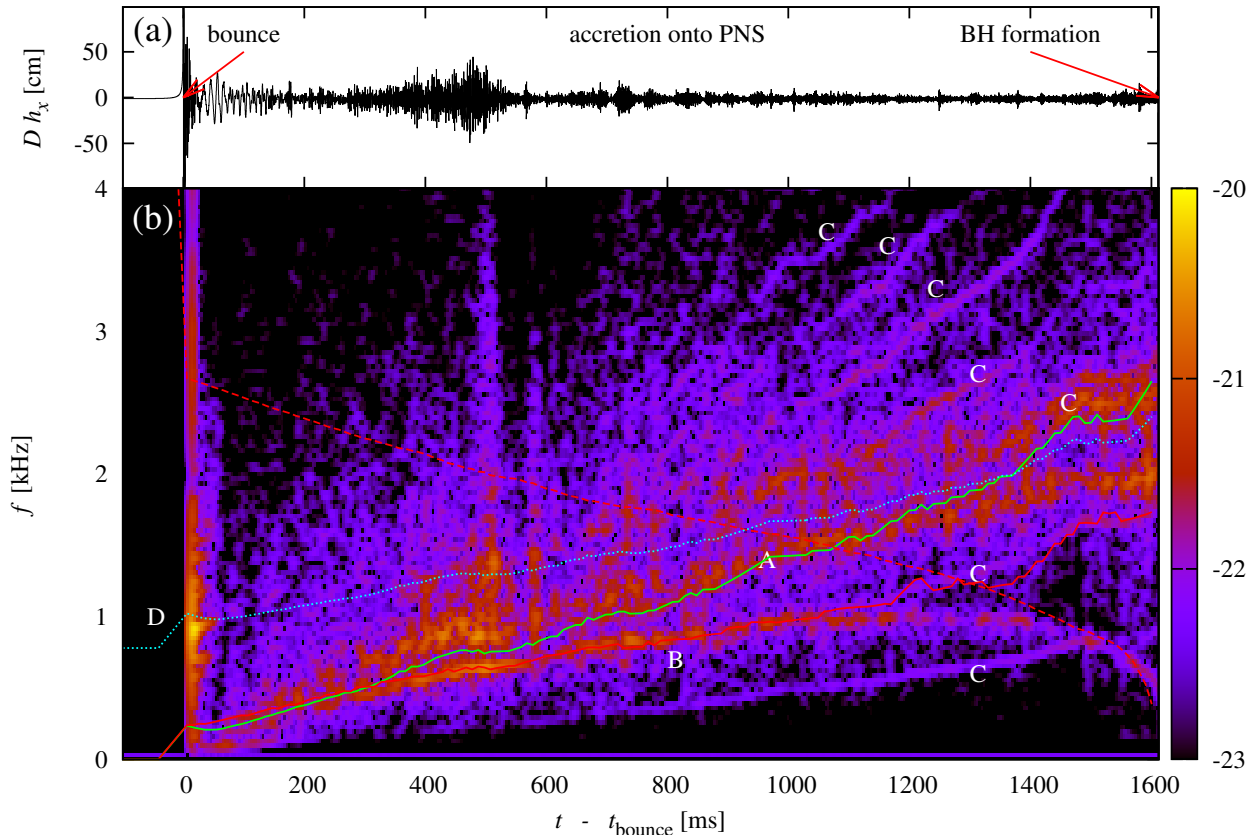


FIG. 3.— Waveform (a) and spectrogram (b) of the characteristic gravitational wave signal for the *fiducial model* at  $D = 100$  kpc. We overplot estimates for the frequency evolution of g-modes at the surface of the PNS (solid-green line), g-modes in the cold inner core (solid-red line), quasi-radial mode (dashed-red line) and f-mode (dotted-blue line). Capital letters point to features described in the main text.

core and its equatorial radius respectively. For the quasi-radial mode we use the results of Gondek et al. (1997) which provide the dependence of the frequency of the radial mode as a function of the central rest mass density,  $\rho_c$ , for PNS models with the LS220 EoS and constant profiles of  $Y_e = 0.4$  and  $s = 2k_b$ . We use a simple fit to this profile, which agrees within  $\sim 20\%$  below 4 kHz, as a rough estimate for the frequency of our PNS:

$$f_{qr} \sim 3.3 \sqrt{\log \rho_{c,BH} - \log \rho_c} \text{ kHz}. \quad (3)$$

Since our rotating model collapses to a BH at a higher central density than the non-rotating model of Gondek et al. (1997), we use the value for the central density at BH formation,  $\rho_{c,BH}$ , of our simulation. We find that (2) and (3) (solid and dashed red lines in Figure 3b, respectively) agree quite well with the observed behaviour of feature “B” and explain naturally the turning point in frequency at  $\sim 1200$  ms after bounce as an avoided crossing and the zero-frequency limit at BH formation.

Comparing the spectrogram of the time evolution of the shock location with Figure 3, there is a close correlation with the features labeled “C”. Our interpretation is that the SASI modes in the shock induce sound waves that travel downwards and excite the PNS surface, which becomes a strong emitter of GWs.

It is also plausible that the feature “D” corresponds to

a f-mode excited at bounce, which then damps quickly due to the strong interaction through sound-waves with the surrounding hot bubble. The frequencies for the fundamental f-mode can be approximated accurately for a wide range of EoS as (Andersson & Kokkotas 1998)

$$f_f \sim 0.78 + 1.635 \sqrt{\frac{M_{PNS}}{1.4M_\odot} \left(\frac{10 \text{ km}}{R_{PNS}}\right)^3} \text{ kHz}, \quad (4)$$

which agrees with the short-lived oscillation that we find at bounce.

Our *slow rotating model* shows a qualitatively similar behaviour, displaying the same features in the spectrogram, including a mode going to zero frequency at the time of BH formation. The smaller centrifugal support of this model has two effects: i) the BH forms earlier, about 1300 ms after bounce, and ii) the object is more compact, which produces larger GW amplitude with higher frequencies.

Figure 4 shows the characteristic GW spectra for both simulations. These signals could be easily observed by advanced GW detectors up to the Magellanic Clouds, and by third generation detectors up to the Virgo cluster.

## 5. DISCUSSION

Estimates of the GW signal emission in the collapse scenario have been studied by Sekiguchi & Shibata (2005) and Ott et al. (2011). In both cases a simplified



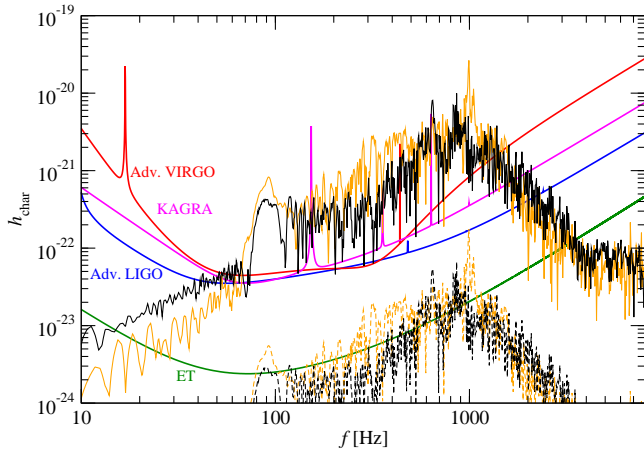


FIG. 4.— Characteristic GW spectra for the *fiducial model* (black lines) and the *slow rotating model* (yellow lines) for sources located at 100 kpc (solid lines) and 15 Mpc (dashed lines), compared with the design sensitivity curves for advanced and planned gravitational wave detectors.

EoS was used, which led to unrealistically short BH collapse times smaller than  $\sim 150$  ms. Their setup skipped the long PNS phase after bounce and the development of the rich GW signal presented in this work, which only appears after the PNS has contracted and the different mode frequencies become distinguishable from one another. We have shown that our longer simulations, which we stop at BH formation for convenience, lead to a long and high-amplitude GW signal with distinctive features providing information about the structure of the PNS and the accretion shock.

The astrophysical objects for which we are computing the GWs and spectra encompass massive, fast-rotating stars, with sub-solar metallicity, that may likely fail to produce energetic supernova explosions. It is currently an active matter of debate what fraction of massive stars produce BHs rather than neutron stars, what

the channels for BH formation are, and what corresponding observational signatures we shall expect (e.g., Lovegrove & Woosley 2013; Piro 2013). Estimating an observational rate for the kind of events at hand is, therefore, involved. Nevertheless, it seems plausible that their rate be a sizable fraction of the failed supernova explosions. Theoretical studies have suggested that the rate of failed SNe is  $\simeq 10\%$  of the core collapse SN rate at solar metallicity (Woosley et al. 2002). More recent estimates based on one dimensional simulations of large amounts of progenitor stars, though excluding rotation and binary effects, rise such a fraction to  $\lesssim 25\%$  (Zhang et al. 2008; Ugliano et al. 2012). From the observational point of view, Horiuchi et al. (2011) identify the so-called “supernova rate problem”, namely that the SN rate predicted from the star formation rate is higher than the SN rate measured by SN surveys. Applied to the very local Universe ( $\lesssim 10$  Mpc), the rate of dim core-collapse SNe is high ( $\sim 30\% - 50\%$ ), and Horiuchi et al. (2011) suggest that it is very likely that a non-negligible fraction of such dim events are associated with core-collapse events producing BHs. Kochanek (2013) suggests that the paucity of observed high mass red supergiants in the range  $16.5M_{\odot} \lesssim M \lesssim 25M_{\odot}$  can be explained if they die as failed supernovae. Such events can account for up to  $\simeq 20\%$  of core collapse SN, i.e., they might be produced at rates  $\sim 0.2 \text{ y}^{-1}$ . Observations indicate that  $10\% - 50\%$  of massive main-sequence stars may be fast spinning objects with rotational velocities  $\gtrsim 200 \text{ km s}^{-1}$  (Mink et al. 2013). Therefore, fast spinning, moderate-metallicity, massive stars as the ones considered in this *Letter*, happening in nearby galaxies, might bring detectable GW signals for the Einstein Telescope at rates of up to  $\sim 0.1 \text{ y}^{-1}$ .

We acknowledge the support from the grants StG-CAMAP-259276, AYA2010-21097-C03-01, PROMETEO-2009-103 and from the GRISOLIA/2010/030 Fellowships program.

#### REFERENCES

- Andersson, N. and Kokkotas, K. 1998 , Mon. Not. R. Soc., 299, 1059
- Aurière, M. 1982 , Astron. & Astrophys., 109, 301
- Baumgarte, T. W., Stuart, L. S. and Shibata, M. 2000 , Astrophys. J., 528, L29
- Buras, R., Janka, H.-Th., Rampp, M. and Kifonidis, M. 2006 , Astron. & Astrophys., 457, 281
- Chandrasekhar, S. 1964 , Astrophys. J., 140, 417
- Chieffi, A. and Limongi, M. 2013 , Astrophys. J., 764, 21
- Cordero-Carrión, I., Cerdá-Durán, P., Dimmelmeier, H., Jaramillo, J. L., Novak, J. andourgoulhon, E. 2009 , Phys. Rev. D., 79, 024017
- DeBrye, N., Cerdá-Durán, P., Aloy, M. A. and Font, J. A., Proceedings of the Spanish Relativity Meeting 2012, arXiv:1310.6223
- Demorest, P. B., Pennucci, T., Ransom, S. M., Roberts, M. S. E. and Hessels, J. W. T. 2010 , Nature, 467, 1081
- Dimmelmeier, H., Font, J. A. and Müller, E. 2002 , Astron. & Astrophys., 388, 917
- Dimmelmeier, H., Novak, J., Font, J. A., Ibáñez, J. M. and Müller, E. 2005 , Phys. Rev. D, 71, 064023
- Fryer, C. L., Belczynski, K., Wiktorowicz, G., et al. 2012, Astrophys. J., 749, 91
- Galeazzi, F., Kastaun, W., Rezzolla, L. and Font, J. A. 2013 , Phys. Rev. D, 88, 064009
- Gondek, D., Haensel, P. and Zdunik, J. L. 1997 , Astron.& Astrophys., 325, 217
- Gondek, D. and Zdunik, J. L. 1999 , Astron.& Astrophys., 344, 117
- Gourgoulhon, E., Haensel, P. and Gondek, D. 1995 , Astrophys. J., 294, 747
- Horiuchi, S., Beacom, J. F., Kochanek, C. S., et al. 2011, Astrophys. J., 738, 154
- Kaplan, J. D., Ott, C. D., O’Connor, E. P., Kiuchi, K., Roberts, L. and Duez, M. 2013, arXiv:1306.4034v1
- Kochanek, C. S., arXiv:1308.0013
- Kokkotas, K. and Ruoff, J. 2001 , Astron.& Astrophys., 366, 565
- Langer, N. 2012, Annu. Rev. Astro. Astrophys. 50, 107
- Lattimer, J. M. and Swesty, F. D. 1991 , Nucl. Phys. A, 535, 331
- Liebendörfer, M., Rampp, M., Janka, H. T. and Mezzacappa, A. 2005 , Astrophys. J., 620, 840
- Liebendörfer, M. 2005 , Astrophys. J., 633, 1042
- Lovegrove, E., and Woosley, S. 2013, Astrophys. J., 769, id.109
- MacFadyen, A. I. and Woosley, S. E. 1999 , Astrophys. J., 524, 262
- MacFadyen, A. I., Woosley, S. E., and Heger, A. 2001, Astrophys. J., 550, 410
- de Mink, S.E., Langer, N. Izzard, R.G., Sana, H., de Koter, A. 2013, Astrophys. J., 764, id166
- Morrison, I.A., Baumgarte, T.W. and Shapiro, S.L. 2004 , Astrophys. J., 610, 941

- Müller, B., Janka, H.-Th. and Marek, A. 2013 , *Astrophys. J.*, 766, 21
- Murphy, J. W., Ott, C. D. and Burrows, A. 2009 , *Astrophys. J.*, 707, 1173
- Obergaulinger, M. and Janka, T., 2012, *Proceedings of the Astronomum 2011*, ASP Conf. Series. 459, 149
- O'Connor, E. and Ott C D 2010 , *Class. Quant. Grav.*, 27, 114103
- O'Connor, E., and Ott, C. D. 2011, *Astrophys. J.*, 730, 70
- Ott, C.D., Reisswig, C., Schnetter, E. et al. 2011 , *Phys. Rev. L.*, 106, 162203
- Piro, A. L. 2013, *Astrophys. J. Lett.*, 768, L14
- Rosswog, S. and Liebendörfer, M. 2003 , *Mon. Not. R. Soc.*, 342, 673
- Ruffert, M., Janka, H.-T. and Schaefer, G. 1996 , *Astron. & Astrophys.*, 311, 532
- Sekiguchi, Y. and Shibata, M. 2005 , *Phys. Rev. D*, 71, 084013
- Timmes, F. X. and Arnett, D. 1999 , *Astrophys. J. Suppl. Ser.*, 125, 277
- Ugliano, M., Janka, H.-Th., Marke, A., and Arcones, A. 2012, *Astrophys. J.*, 757, 69
- Woosley, S.E. 1993, *Astrophys. J.*, 405, 273
- Woosley, S. E., Heger, A. and Weaver, T. A. 2002 , *Rev. Mod. Phys.*, 74, 1015
- Woosley, S. E. and Heger, A. 2006 , *Astrophys. J.*, 637, 914
- Woosley, S. and Heger, A. 2007 , *Phys. Rep.*, 442, 269
- Woosley, S. E., and Heger, A. 2012, *Astrophys. J.*, 752, 32
- Zhang, W., Woosley, S.E., and Heger, A. 2008, *Astrophys. J.*, 679, 639